Surface energy balance and actual evapotranspiration of the transboundary Indus Basin estimated from satellite measurements and the ETLook model

W. G. M. Bastiaanssen,[1,2] M. J. M. Cheema,[1,3,4] W. W. Immerzeel,[5,6] I. J. Miltenburg,[2] and H. Pelgrum[2]

Received 26 January 2011; revised 3 September 2012; accepted 19 September 2012; published 21 November 2012.

[1] The surface energy fluxes and related evapotranspiration processes across the Indus Basin were estimated for the hydrological year 2007 using satellite measurements. The new ETLook remote sensing model (version 1) infers information on actual Evaporation (E) and actual Transpiration (T) from combined optical and passive microwave sensors, which can observe the land-surface even under persistent overcast conditions. A two-layer Penman–Monteith equation was applied for quantifying soil and canopy evaporation. The novelty of the paper is the computation of E and T across a vast area (116.2 million ha) by using public domain microwave data that can be applied under all weather conditions, and for which no advanced input data are required. The average net radiation for the basin was estimated as being 112 Wm^{-2}. The basin average sensible, latent and soil heat fluxes were estimated to be 80, 32, and 0 Wm^{-2}, respectively. The average evapotranspiration (ET) and evaporative fraction were 1.2 mm d^{-1} and 0.28, respectively. The basin wide ET was 496 ± 16.8 km^3 yr^{-1}. Monte Carlo analysis have indicated 3.4% error at 95% confidence interval for a dominant land use class. Results compared well with previously conducted soil moisture, lysimeter and Bowen ratio measurements at field scale ($R^2 = 0.70$; RMSE = 0.45 mm d^{-1}; RE = –11.5% for annual ET). ET results were also compared against earlier remote sensing and modeling studies for various regions and provinces in Pakistan ($R^2 = 0.76$; RMSE = 0.29 mmd^{-1}; RE = 6.5% for annual ET). The water balance for all irrigated areas together as one total system in Pakistan and India (26.02 million ha) show a total ET value that is congruent with the ET value from the ETLook surface energy balance computations. An unpublished validation of the same ETLook model for 23 jurisdictional areas covering the entire Australian continent showed satisfactory results given the quality of the watershed data and the diverging physiographic and climatic conditions ($R^2 = 0.70$; RMSE = 0.31 mmd^{-1}; RE = –2.8% for annual ET). Eight day values of latent heat fluxes in Heibei (China) showed a good resemblance ($R^2 = 0.92$; RMSE = 0.04 mm d^{-1}; RE = 9.5% for annual ET). It is concluded that ETLook is a novel model that can be operationalized further—especially after improving the preprocessing of spaceborne soil moisture data. This preprocessing includes (1) downscaling of topsoil moisture from 25 to 1 km pixels, and (2) translation of topsoil moisture into subsoil moisture values.

Citation: Bastiaanssen, W. G. M., M. J. M. Cheema, W. W. Immerzeel, I. J. Miltenburg, and H. Pelgrum (2012), Surface energy balance and actual evapotranspiration of the transboundary Indus Basin estimated from satellite measurements and the ETLook model, *Water Resour. Res.*, *48*, W11512, doi:10.1029/2011WR010482.

[1]Water Management Department, Faculty of Civil Engineering and Geosciences, Delft University of Technology, Delft, Netherlands.
[2]eLEAF Competence Center, Wageningen, Netherlands.
[3]Department of Irrigation and Drainage, University of Agriculture, Faisalabad, Pakistan.
[4]International Water Management Institute, Lahore, Pakistan.
[5]FutureWater, Wageningen, Netherlands.
[6]Department of Physical Geography, University of Utrecht, Utrecht, Netherlands.

Corresponding author: M. J. M. Cheema, Department of Irrigation and Drainage, University of Agriculture, Faisalabad, Pakistan. (mjm.cheema@gmail.com)

0043-1397/12/2011WR010482

1. Introduction

[2] Planning and monitoring of consumptive water use is necessary for sound management of scarce water resources. Consumptive use influences social, economic, agricultural, and environmental development. Water is consumed mainly through evaporation (E) and transpiration (T) (jointly termed evapotranspiration (ET)) from crops, soil, forests, urban areas, and natural vegetation, among others. If precipitation over a specific land cover exceeds ET (e.g., forests), such a land cover class is a net producer of water resources. Non-consumed water from precipitation feeds streams, rivers and aquifers. If, however, ET exceeds precipitation, such a land cover class will be a net consumer of water resources.

Irrigated lands are a typical example of a net consumer of water. ET information can be used for irrigation management [*Allen et al.*, 2007; *Bastiaanssen et al.*, 1996], drought detection [e.g., *Calcagno et al.*, 2007], real water savings [e.g., *Seckler*, 1996], water accounting [e.g., *Molden and Sakthivadivel*, 1999], water productivity [e.g., *Zwart et al.*, 2010], virtual water trade [e.g., *de Fraiture and Wichelns*, 2010], model calibration [e.g., *Immerzeel and Droogers*, 2008], hydrological model applications [*Droogers et al.*, 2010] and groundwater management [*Ahmad et al.*, 2005].

[3] A number of techniques are in use to measure ET, ranging from conventional point measurements to modeling and spatially distributed remote sensing estimates. At individual plant and field scales, lysimeters, heat pulse velocity, Bowen ratio, scintillometry, surface renewal, and eddy correlation are commonly used [e.g., *Meijninger et al.*, 2002; *Nagler et al.*, 2005]. Field scale ET measurements are generally considered accurate, however the accuracy of these traditional methods is often less than 90% [*Teixeira and Bastiaanssen*, 2012; *Twine et al.*, 2000]. The equipment cost, extensive labor, and coverage issues restrict use of these techniques at large scale [*Elhaddad and Garcia*, 2008]. At the regional scale, earth observations by means of satellite data are gradually becoming more accepted [e.g., *Anderson et al.*, 2007; *Courault et al.*, 2005; *Guerschman et al.*, 2009; *Kalma et al.*, 2008; *Mu et al.*, 2007; *Wu et al.*, 2012] although operational data provision remains rare. This paper aims at contributing to the development of operational systems that could be applied on a daily time step for areas with limited ground data. Routine weather data is assumed to be available.

[4] Evapotranspiration computations are often based on surface energy balances [e.g., *Long and Singh*, 2012; *Mu et al.*, 2007; *Price*, 1990; *Senay et al.*, 2007; *Tang et al.*, 2009]. Many of these energy balance models require thermal infrared radiation from cloud free images and atmospheric corrections in order to produce accurate land surface temperature maps [*Jia et al.*, 2009]. Cloud free surface temperature images for large areas in basins with monsoon climates are not straightforward to obtain [e.g., *Bastiaanssen and Bandara*, 2001]. Thermal infrared radiation is more sensitive to atmospheric water vapor absorption than visible and near-infrared radiation [*Lillesand and Kiefer*, 2000], and it is thus more challenging to acquire land surface temperature maps not being thwarted by clouds. For instance, the surface temperature product (MOD 11A2) available through Moderate Resolution Imaging Spectro radiometer (MODIS) is thwarted by cloud cover for the entire period of monsoon 2007 (June–September). About 50% of the basin area was found without or with limited surface temperature data from day of year (DOY) 161 to 241. This illustrates the difficulty in getting continuous information for ET computations in irrigated areas from thermal infrared data. While it is generally accepted that thermal infrared data provide reliable results based on sound physics [e.g., *Allen et al.*, 2011; *Allen et al.*, 2010; *Bastiaanssen et al.*, 2008], the cloud cover is a serious hindrance to routine applications in various parts of the world.

[5] To circumvent these problems, the current study deployed the first version of the ETLook algorithm. Soil moisture derived from passive microwave sensors is the driving force for calculation of the surface energy balance in ETLook. Surface soil moisture relates typically to a depth of 2 to 3 cm, and the number of surface soil moisture databases is growing due to an increasing number of operational passive microwave sensors. The accuracy and spatial resolution are expected to improve in the near future. Future soil moisture data layers will be based on active Synthetic Active Radar (SAR) measurements, once this data become available easily and free of charge. This is a good moment to explore and develop ET models that are based on soil moisture data sets.

[6] Microwave radiometry is less affected by cloud cover [*Fily et al.*, 1995; *Ulaby et al.*, 1981] and can thus provide continuous surface soil moisture information even in monsoon periods. *Li et al.* [2006] have shown the value of using microwave derived near-surface soil moisture in a two-source energy balance model over an agricultural area in central Iowa (USA). The ETLook algorithm is a two-source model and surface soil moisture is used for the computation of E, and a parameterization is introduced to compute subsoil moisture content for the determination of T.

[7] Accurate ET information is of paramount importance for the 116.2 million hectares (mha) Indus Basin, with high elevation water source areas, a distinct monsoon climate with cloud covered regions, and declining water tables due to over-exploitation. This study was a first attempt to use microwave technologies to accurately estimate ET over the Indus Basin, and to detect areas with excessively high ET rates using a spatial resolution of 1 km. Such a resolution is thought to be good enough for regional-scale applications. The main objective of this study was to demonstrate the validity of a combined optical and microwave based energy balance model (ETLook) in a vast river basin with large irrigation systems. Another objective was to use public domain data to estimate ET in the areas where field data are not available, and to show water managers that spatially discrete ET information is the basis for describing the major water flowpath in ungauged basins.

2. Study Area

[8] The study area is the Indus Basin, which lies between latitude 24°38′ to 37°03′N and longitude 66°18′ to 82°28′E. The total area of the basin is 116.2 mha and encompasses four countries (Pakistan: 53%, India: 33%, China: 8% and Afghanistan: 6%) (Figure 1). The basin exhibits complex hydrological processes due to variability in topography, rainfall, and land use. The elevations range from 0–8611 m above mean sea level (a.m.s.l) and mean annual rainfall varies between approximately 200 to 1500 mm. The basin-wide average rainfall for 2007 was 383 mm yr^{-1} [*Cheema and Bastiaanssen*, 2012]. The basin has two distinct agricultural seasons, being the wet *kharif* monsoon season (May to October) and the dry *rabi* season (November to April). Wheat is the major *rabi* crop while rice and cotton are major *kharif* crops. Irrigated agriculture is practiced in 26.02 mha (22.6% of total basin area) area of the basin (see Figure 1). The irrigation system in the Indus Basin supplies surface water to the middle and lower parts. The era of tube-well installations with subsidized rates and direct access to water has motivated farmers to augment shortages in surface water with groundwater resources [*Shah et al.*, 2000].

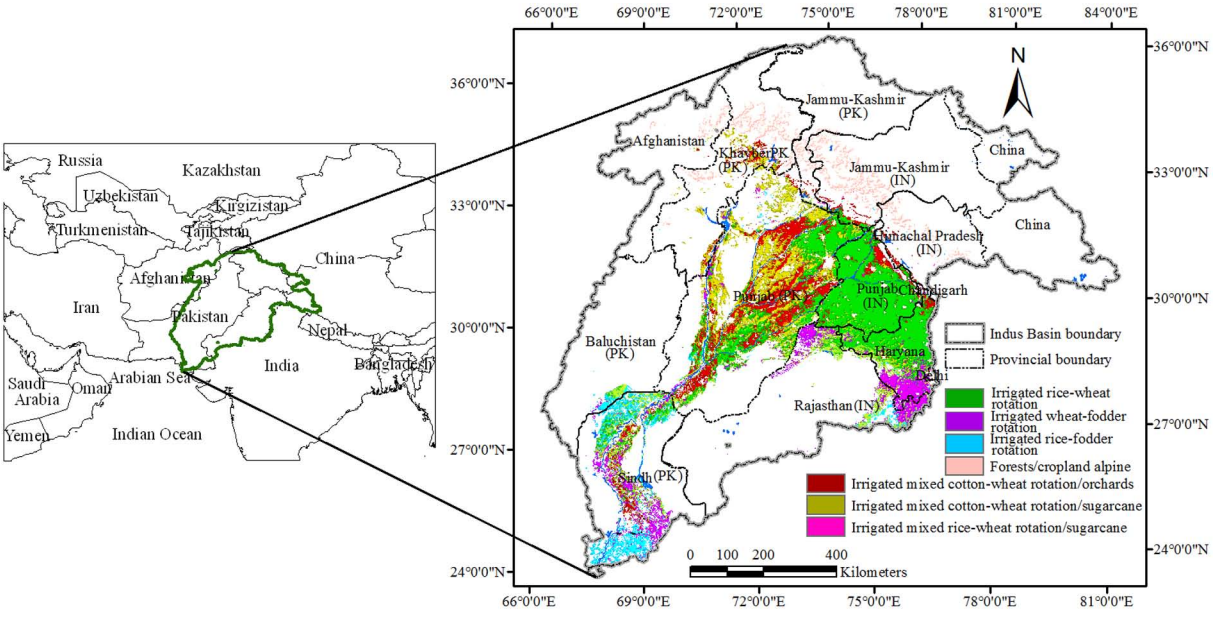

Figure 1. Location of the Indus Basin and provinces of different countries in the basin. PK stands for Pakistan and IN for India. The irrigated areas in the basin are also shown. [from *Cheema and Bastiaanssen*, 2010].

Currently 40–50% of agricultural water needs are met through groundwater used in conjunction with surface water [*Sarwar and Eggers*, 2006].

3. Material and Methods

3.1. Satellite Data and Preprocessing

[9] Key input data for ETLook are: surface soil moisture, spectral vegetation index, surface albedo, atmospheric optical depth, land use and land cover (LULC), soil physical properties, and meteorological data. Surface soil moisture was obtained from the Advanced Microwave Scanning Radiometer (AMSR-E) on the Aqua satellite. Daily soil moisture datasets with 25 km foot print (ascending and descending path) covering the Indus Basin were downloaded from the National Snow and Ice Data Center (NSIDC) website (see http://nsidc.org/data/ae_land3.html) for the complete year of 2007 [*Njoku*, 2008]. The year 2007 was selected because all required auxiliary data were available. The actual spatial resolution of C-band AMSR-E soil moisture is large (approximately 70 km × 40 km). AMSR-E collects 60 km resolution C-band brightness temperature with a sampling interval of 10 km, which allows AMSR-E C-band data to be gridded at 25 km resolution. The operational character of surface soil moisture in NSIDC contributes to the construction of a routine provision of spatial ET data bases. A comprehensive soil moisture data validation study in the Indus Basin was performed by *Cheema et al.* [2011]. The soil moisture data was validated against rainfall, vegetation and saturated water content. The soil moisture has shown strong relationship with rainfall and vegetation. It was found that both the behavior as well as the absolute values of topsoil moisture are realistic and provide sufficient information on the spatial and temporal changes of topsoil moisture in the Indus Basin. The daily layers were in the current study averaged to obtain 8-day soil moisture layers to be compatible with the MODIS optical satellite data.

[10] This Indus Basin ETLook study required topsoil moisture at 1 km scale, while the data is provided at 25 km scale. Various sophisticated methods are documented in the literature to downscale the available coarse resolution soil moisture data to 1 km pixels [*Friesen et al.*, 2008; *Gharari et al.*, 2011; *Hemakumara et al.*, 2004; *Merlin et al.*, 2006, 2008]. All these downscaling methods require a number of parameters and have an empirical character related to the physiographical setting of a specific area. More research studies are required to find more generic solutions to this problem, and it is outside the scope of this paper to compare and validate all these methods. Due to the absence of detailed soil moisture data in the Indus Basin, a simple method of downscaling based on effective saturation has been adopted in this study. Each AMSR-E pixel was downscaled to 1 km using a bilinear resampling technique first. This is simplistic, but is necessity to remove abrupt changes in the data layers due to the texture of the large-scale AMSR-E pixels. The information on saturated and residual moisture content (θ_{sat} and θ_{res}, respectively) for each soil type was used to calculate topsoil effective saturation $\left(S_{e,xy}^{top}\right)$ at 1 km grid using the definition proposed by *van Genuchten* [1980] as:

$$S_{e,xy}^{top} = \frac{\theta_{AMSRE} - \theta_{res,xy}}{\theta_{sat,xy} - \theta_{res,xy}}, \quad (1)$$

where $S_{e,xy}^{top}$, θ_{AMSRE}, $\theta_{sat,xy}$, and $\theta_{res,xy}$ represent the effective saturation, AMSRE soil moisture, saturated and residual moisture content at 1 km pixel (x,y), respectively. The values for $\theta_{sat,xy}$ and $\theta_{res,xy}$ were inferred from the Food and Agriculture Organization (FAO) soil map [*FAO*, 1995] using pedo-transfer functions (P. Droogers, unpublished data, 2006). The minimum and maximum values of a particular

pixel or geographic area has not been used because it cannot be certified that these very extreme end points do ever occur. Soils with a large pore volume (θ_{sat}) contain more air and have a lower degree of saturation. Their drier conditions reduce soil evaporation because soil moisture is retained stronger to the soil matrix, and the volume with water filled pores that are needed to transport water will be lower under dry conditions. While being simplistic, a scaling with θ_{sat} has certain merits.

[11] In addition, the saturation of the subsoil $\left(S_e^{sub}\right)$ is required for the computation of root water uptake and subsequent crop transpiration. The preprocessing of saturation of the subsoil was done by using an empirical relationship between S_e^{top}, the vegetation photosynthetical activity (that reflect soil water availability with a certain lag time) and S_e^{sub}. The following relationship is imbedded in ETLook1.0 and was applied in the current study:

$$S_e^{sub} = 0.1\text{LAI} + (1 - 0.1\text{LAI})[1 - \exp\{S_e^{top}(-0.5\text{LAI} - 1)\}], \quad (2)$$

where LAI is the Leaf Area Index. The basic assumption is that the degree of saturation of the subsoil exceeds the saturation of the topsoil when vegetation is photosynthetically active, and that S_e^{top} affects the level of S_e^{sub} under all conditions. The green LAI reflects the access of vegetation to soil water across a longer period. Since it is based on spectral leaf reflectances, LAI represents the real state conditions of the canopy, including its leaf water content, among others. The LAI does not reflect the daily moisture conditions of the canopy and the subsoil, the day-to-day variability of S_e^{sub} is therefore entirely regulated by S_e^{top}. In absence of green plants, moisture in the subsoil holds a direct analytical relationship with the moisture in the topsoil [e.g., *Hillel*, 1998]. Hence, passive microwave data in combination with LAI describes the daily variation of root zone soil water content.

[12] The Normalized Difference Vegetation Index (NDVI) is an undisputed indicator of active vegetation and was used to compute LAI as explained further down. It has been demonstrated by, for instance *Nagler et al.* [2005] and *Burke et al.* [2001], that NDVI is an indicator of ET fluxes, which is in line with equation (2). NDVI data are distributed by the Land Processes Distributed Active Archive Center (LP DAAC), located at the U.S. Geological Survey (USGS) Earth Resources Observation and Science (EROS) Center (see lpdaac.usgs.gov). Two 16-day NDVI datasets (MOD13A2 and MYD13A2 (collection 5) starting from day 1 and day 9, respectively) at 1 km were used to create 8-day NDVI layers. The vegetation cover (VC) was derived from NDVI following *Jiang et al.* [2006] as:

$$\text{VC} = 1 - \left(\frac{\text{NDVI}_{fv} - \text{NDVI}}{\text{NDVI}_{fv} - \text{NDVI}_{bs}}\right)^{0.7}. \quad (3)$$

[13] Threshold values of NDVI = 0.8 and 0.125 were used as boundary condition for full vegetation cover (NDVI_{fv}) and bare soil (NDVI_{bs}), respectively. The LAI was computed from NDVI values using standard asymptotic relationships between LAI and VC [e.g., *Carlson and Ripley*, 1997; *Curran and Steven*, 1983]:

$$\text{LAI} = -\ln[(1 - \text{VC})/a], \quad (4)$$

where a is the light extinction coefficient with a value range of 0.40 to 0.65. An average value of 0.5 was taken for all representative vegetation types [e.g., *Kale et al.*, 2005]. The LAI (VC) relationship was similar for all land use classes because a values for all classes were not available and we assumed that a differences between classes were small enough to justify the use of a few selective a values, for all classes.

[14] Surface albedo was also derived from standard MODIS products. The 8-day albedo data product MCD43B3 (collection 5) at 1 km resolution was downloaded from (see https://wist.echo.nasa.gov/~wist/api/imswelcome/) server provided by LP DAAC.

[15] Solar radiation is classically computed from the extraterrestrial radiation in association with an atmospheric transmissivity in the solar spectrum. The atmospheric transmissivity of shortwave radiation can be inferred from optical depth information provided by the MODIS cloud product [*King et al.*, 1997]. One km resolution MYD06_L2 values of the optical depth product were downloaded from https://wist.echo.nasa.gov/~wist/api/imswelcome/ to estimate atmospheric transmissivity for the Indus Basin. The cloud optical depth from the MODIS products was used to infer atmospheric transmissivity of shortwave radiation τ_{MODIS} [*Barnard and Long*, 2004].

[16] A detailed Land Use and Land Cover (LULC) map of the Indus Basin developed by *Cheema and Bastiaanssen* [2010] was used to infer information on different LULC classes in the basin. Twenty-seven LULC classes were identified. This LULC classification was used to create look-up tables for the definition of certain bio-physical parameters required for ET computations, such as minimum stomatal resistance, moisture sensitivity and maximum obstacle height.

[17] Rainfall (R) data are used to determine interception evaporation. Interception (I) is computed on a daily scale with the classical von Hoyningen model following *von Hoyningen-Hune* [1983] and *Braden* [1985].

$$\text{I} = 0.2\text{LAI}\left[1 - \left(\frac{1}{1 + \frac{(\text{VC})\text{R}}{0.2\text{LAI}}}\right)\right], \quad (5)$$

which assumes that maximum a water film of 0.2 mm is stored per unit LAI. This coefficient can be modified. ET cannot exceed R without being augmented by additional water resources. Rainfall is therefore a good measure to validate ET of natural vegetation against. By absence of sufficient rain gauges, rainfall was obtained at spatial resolution of 25 km using Tropical Rainfall Measuring Mission (TRMM) processing algorithms described by *Huffman et al.* [2007]. The global rainfall algorithm (3B43 V6) available through NASA website (see http://neo.sci.gsfc.nasa.gov/Search.html?group=39) was used. It provides monthly accumulated rainfall data, which has been calibrated and validated according to the Geographical Differential Analysis (GDA) as outlined in *Cheema and Bastiaanssen* [2012].

3.2. Meteorological Data

[18] The major portion of the Indus Basin (53%) lies within the administrative boundaries of Pakistan. Most of the

meteorological data (e.g., air temperature, relative humidity and wind speed) were therefore obtained from 65 meteorological stations under the aegis of the Pakistan Meteorological Department (PMD). Weather station data for India, China and Afghanistan were extracted from the National Oceanic and Atmospheric Administration (NOAA) National Climatic Data Center (NCDC). The NCDC collects meteorological data from real time reporting stations worldwide in agreement with World Meteorological Organization regulations (ftp://ftp.ncdc.noaa.gov/pub/data/gsod/). Data from 16 stations with complete datasets were downloaded. Hence, air temperature, relative humidity and wind speed data from 81 stations collected at standard height of 2 m were obtained.

[19] ETLook requires gridded meteorological data for air temperature (T_{air}), relative humidity (RH) and wind speed (U_2) at 1 km resolution. Topography, land use, sun angle, and distance from water bodies directly affects the spatial variability of near surface meteorological parameters [*Brutsaert*, 1982; *Schulze et al.*, 1993]. Ordinary geospatial interpolation techniques do not take these variables into account. The meteorological distribution model (Daymet) described by *Thornton et al.* [1997] was therefore used to convert point data to spatial meteorological data. Daymet uses a truncated Gaussian weighting filter for regional distribution of climatic variables in relation with topography. A 1 km Digital Elevation Model (DEM) obtained from GTOPO30 database (see http://eros.usgs.gov/#/Find_Data/Products_and_Data_Available/gtopo30_info) was used to establish relationships between the climatic variables and topography.

[20] The weather grids for 2007 were independently validated against values from the International Water Management Institute (IWMI) world water and climate atlas that is based on long-term field measurements and specific spatial interpolation procedures (http://www.iwmi.cgiar.org/WAtlas/Default.aspx). The atlas provides monthly summaries of rainfall, temperature, humidity, wind speed, and sun shine hours at 18 km grid averaged over the period 1961–1990, as produced by the University of East Anglia [*New et al.*, 1999]. The 8-day Daymet estimates were aggregated to monthly values in order to make them comparable with the IWMI atlas. A high coefficient of determination ($R^2 > 0.85$) was obtained for air temperature estimates. However, for relative humidity and wind speed, moderate coefficients of determination (R^2 = 0.70–0.80 and 0.60–0.70, respectively) were achieved. These correlations are considered reasonable because IWMI atlas values are monthly averages for 1961–1990, which may be different for different years. The IWMI atlas values are also interpolated and extrapolated, and associated with a certain uncertainty. Nevertheless, the impression is that air humidity and wind speed values display more uncertainty than air temperature.

3.3. Theoretical Background of ETlook

[21] The surface energy balance can be written as:

$$R_n - G = \lambda E + H \qquad (\mathrm{Wm^{-2}}), \tag{6}$$

where R_n is net radiation, G is soil heat flux, λE is latent heat flux and H is the sensible heat flux. λE is associated with ET. The ETLook algorithm uses a two layer approach to solve the Penman–Monteith equation. The Penman–Monteith equation for E and T can be written as:

$$\mathrm{E} = \frac{\Delta(R_{n,\mathrm{soil}} - G) + \rho c_p \left(\frac{\Delta_e}{r_{a,\mathrm{soil}}}\right)}{\Delta + \gamma\left(1 + \frac{r_{\mathrm{soil}}}{r_{a,\mathrm{soil}}}\right)}, \tag{7}$$

$$\mathrm{T} = \frac{\Delta(R_{n,\mathrm{canopy}}) + \rho c_p \left(\frac{\Delta_e}{r_{a,\mathrm{canopy}}}\right)}{\Delta + \gamma\left(1 + \frac{r_{\mathrm{canopy}}}{r_{a,\mathrm{canopy}}}\right)}, \tag{8}$$

where E and T are evaporation and transpiration, respectively, in $\mathrm{Wm^{-2}}$; Δ (mbar $\mathrm{K^{-1}}$) is the slope of the saturation vapor pressure curve, which is a function of air temperature (T_{air}, °C) and saturation vapor pressure (e_s, mbar); Δ_e(mbar) is vapor pressure deficit, which is the difference between the saturation vapor content and the actual vapor content; ρ (kg $\mathrm{m^{-3}}$) is the air density, and c_p is specific heat of dry air = 1004 J $\mathrm{kg^{-1}\ K^{-1}}$; γ (mbar $\mathrm{K^{-1}}$) is the psychometric constant; $R_{n,\mathrm{soil}}$ and $R_{n,\mathrm{canopy}}$ are the net radiations at soil and canopy, respectively; r_{soil} and r_{canopy} are resistances of soil and canopy, while $r_{a,\mathrm{soil}}$ and $r_{a,\mathrm{canopy}}$ are aerodynamic resistances for soil and canopy, respectively. All resistances are in s $\mathrm{m^{-1}}$. The E and T fluxes (W $\mathrm{m^{-2}}$) are converted to rates (mm $\mathrm{d^{-1}}$) using a temperature-dependent function of the latent heat of vaporization.

[22] The LAI can be used to partition the net radiation into net radiation of the soil ($R_{n,\mathrm{soil}}$) and the canopy ($R_{n,\mathrm{canopy}}$) [*Shuttleworth and Wallace*, 1985]. The increase in LAI results in an exponential decrease in the fraction of radiation available for the soil, and vice versa for the canopy. The energy dissipation due to interception losses is subtracted from the total net radiation. This energy is computed from the actual interception evaporation rates and the latent heat of vaporization being associated with that. The net radiation at the soil and canopy can be calculated using Beer's law as follows:

$$R_{n,\mathrm{soil}} = \{(1 - \alpha_o)R^{\downarrow} - L_n - I\}\exp(-a\mathrm{LAI}), \tag{9}$$

$$R_{n,\mathrm{canopy}} = \{(1 - \alpha_o)R^{\downarrow} - L_n - I\}\{1 - \exp(-a\mathrm{LAI})\}, \tag{10}$$

where α_o is surface albedo (–); $R^{\downarrow}$ ($\mathrm{Wm^{-2}}$) is the incoming shortwave radiation; L_n, ($\mathrm{Wm^{-2}}$) is the net longwave radiation; I is the interception of water by leaves expressed in $\mathrm{Wm^{-2}}$; and a is the light extinction coefficient for net radiation. The incoming shortwave radiation can be calculated using daily measurements of shortwave transmissivity (τ_{sw}) and the theoretical extraterrestrial radiation (R_{toa}). The parameterization for $R^{\downarrow}$ and L_n, is taken from the FAO Irrigation and Drainage Paper 56 [*Allen et al.*, 1998]. The sum of $R_{n,\mathrm{soil}}$ and $R_{n,\mathrm{canopy}}$ constitute total net radiation R_n, after being corrected for interception losses.

[23] The surface resistances in equations (7) and (8) describe the influence of the soil on evaporation or canopy transpiration. The soil resistance (r_{soil}) is a function of the

topsoil effective saturation (S_e^{top}), estimated using equation (1). A power function defines this relationship [e.g., *Camillo and Gurney*, 1986; *Clapp and Hornberger*, 1978; *Dolman*, 1993; *Wallace et al.*, 1986]:

$$r_{soil} = b(S_e^{top})^c, \tag{11}$$

where b and c are soil resistance parameters, which can vary with soil type and are taken here as 30 and –3, respectively. The coefficients b and c can be calibrated under local conditions if more information is available, such as monthly rainfall amounts and detailed soil maps.

[24] Canopy resistance describes the resistance of vapor flow through the transpiring vegetation and is a function of the minimum stomatal resistance $r_{s,min}$ (s m^{-1}), in association with a number of reduction factors and the leaf area.

[25] The canopy resistance under actual growing conditions can be computed using the common Jarvis-Stewart parameterization [*Jarvis*, 1976; *Stewart*, 1988]. The Jarvis-Stewart parameterization is common in many soil-vegetation-transfer models. It describes the joint response of soil moisture and LAI on transpiration fluxes in a biophysically justified manner. The Jarvis-Stewart parameterization describes the response of stomata to environmental factors in the form of minimal resistance multiplied by the product of interacting stresses on plants, and is computed as follows:

$$r_{canopy} = \left(\frac{r_{s,min}}{LAI_{eff}}\right)\left(\frac{1}{S_t S_v S_r S_m}\right), \tag{12}$$

where S_t is temperature stress, and a function of minimum, maximum and optimum temperatures, as defined by *Jarvis* [1976]; S_v is vapor pressure stress induced due to persistent vapor pressure deficit; S_r is radiation stress induced by the lack of incoming shortwave radiation; and S_m is soil moisture stress originating from the root zone. S_m is defined using a sinusoidal relationship with sub soil effective saturation (S_e^{sub}) and tenacity factor (K_{sf}) defined in *American Society of Civil Engineers* (*ASCE*) [1996] as:

$$S_m = K_{sf} S_e^{sub} - \frac{\sin(2\pi S_e^{sub})}{2\pi}, \tag{13}$$

where K_{sf} describes the ability of plants to extract soil moisture under different moisture conditions. It ranges from 1 for sensitive plants to 1.5 for moderately sensitive plants to 3 for insensitive (tenacious) plants. The value $r_{s,min}$ represents the resistance to transpiration from canopy under ideal conditions (no moisture stress, enough sunshine etc.). The resistance $r_{s,min}$ can have different values for the different land use classes. The $r_{s,min}$ is defined for a single layer of leaves, therefore effective leaf area index LAI_{eff}, which describes the actual transpiring leaf mass, was used for integration from leaf to canopy. The leaf area integrates the vaporization process from leaf to canopy scale. The following equation, as described by *Mehrez et al.* [1992] and *Allen et al.* [2006], was used to infer LAI_{eff}:

$$LAI_{eff} = \frac{LAI}{0.3LAI + 1.2}. \tag{14}$$

[26] The aerodynamic resistance for soil ($r_{a,soil}$) and canopy ($r_{a,canopy}$) can be computed [*Allen et al.*, 1998; *Choudhury et al.*, 1986; *Holtslag*, 1984] as:

$$r_{a,soil} = \frac{\ln\left(\frac{z_{obs}}{z_{0,soil}}\right)\ln\left(\frac{z_{obs}}{0.1z_{0,soil}}\right)}{k^2 u_{obs}}, \tag{15}$$

$$r_{a,canopy} = \frac{\ln\left(\frac{z_{obs}-d}{z_{0,m}}\right)\ln\left(\frac{z_{obs}-d}{0.1z_{0,m}}\right)}{k^2 u_{obs}}, \tag{16}$$

where k is von Karman constant = 0.41[-], u_{obs} is the wind speed at observation height [ms^{-1}], d is displacement height [m], $z_{0,soil}$ is the soil surface roughness, $z_{0,m}$ is the surface roughness. The land use map is used to prescribe values for $z_{0,m}$. Bare soil has been assigned with a value of $z_{0,soil}$ being 0.001 m. Research is in progress to derive surface roughness from radar imagery, and it is expected that backscatter coefficients can describe roughness in the near future.

[27] The soil heat flux (G) for land surface is calculated using a sine function as described by *Allen et al.* [1998]. The maximum value for G is recorded in May for northern latitudes, which coincides with a phase of $-\pi/4$. For southern latitudes the phase is $-\pi/4 + \pi$.

$$G = \frac{\sqrt{2}A_{t,year}k\sin\left(\frac{2\pi J}{P} - \frac{\pi}{4}\right)}{z_d}\exp(-a\mathrm{LAI}), \tag{17}$$

where $A_{t,year}$ is the yearly amplitude for air temperature; J is the Julian day measured in seconds; k is the soil thermal conductivity (W m^{-1} K^{-1}), which has a linear relationship with topsoil moisture; a is the same light extinction coefficient as used in Beers law, see equations (9) and (10); z_d (m) is the damping depth that is calculated as:

$$z_d = \sqrt{\frac{2kP}{2\pi\rho c_p}}, \tag{18}$$

where P is the period in seconds; and ρc_p is the volumetric heat capacity (a function of the porosity and S_e^{top}). Equation (17) includes light interception effects on soil heat flux.

3.4. Calibration and Validation Approaches

[28] The cloud optical depth measures the attenuation of solar radiation passing through the atmosphere due to scattering and absorption by cloud droplets. The cloud optical depth can be defined as the negative algorithm of the fraction of the incoming radiation that is not scattered or absorbed in the atmosphere [*Kitchin*, 1987]. Maximum and minimum threshold atmospheric transmissivity values were taken into consideration to account for latitude, zenith angle and diffuse radiation. The resulting atmospheric transmissivity (τ_{MODIS}) was checked and calibrated using the simplified—but doable—field methods suggested by *Angstrom* [1924] and *Hargreaves and Samani* [1985]. Records of sunshine hours were used for the Angstrom equation. Sunshine records were available from 24 stations in the study area. The same 24 stations were used to get diurnal air temperature

differences for the Hargreaves equation. Results from the Angstrom and Hargreaves methods were used to determine a linear fit through the origin for each time interval of 8 days, to obtain calibrated shortwave transmissivity (τ_{sw}):

$$\tau_{sw} = e.\tau_{MODIS}, \tag{19}$$

where e is the regression coefficient.

[29] Minimum stomatal resistance values $r_{s,\min}$ for each LULC were used to fine-tune ETLook. The $r_{s,\min}$ values for agricultural classes were accepted to be between 40 to 140 s m^{-1} [*ASCE*, 1996; *Bastiaanssen and Bandara*, 2001; *Radersma and de Ridder*, 1996]. Various researchers [e.g., *Allen et al.*, 1998; *Monteith*, 1981; *Sharma*, 1985; *Vanderkimpen*, 1991] suggested a value of $r_{s,\min} = 100$ s m^{-1} for various agricultural crops like wheat, rice, beans, etc. First, this default $r_{s,\min}$ value was used for all agricultural classes ($n = 11$). The following values were assigned to the remaining classes: pastures 125 s m^{-1}, savannas 150 s m^{-1}, forests 150 and 300 s m^{-1}(for broadleaf and needleleaf forests, respectively), sparse vegetation 200 s m^{-1}, and urban and industrial settlements 60 s m^{-1}. Water bodies were assigned 0 s m^{-1} because water vapor molecules can be transported into the atmosphere without physical barriers. During the second run of ETLook, all LULC classes with irrigated crops were assigned 80 s m^{-1} and the rainfed crops were assigned a value of 150 s m^{-1}. During the third run, adjustments were made to the urban and industrial settlements land use, and a $r_{s,\min}$ value of 500 s m^{-1} was assigned.

[30] The ET output data cannot be used for water resources management without testing its accuracy. Results from previous studies based on soil moisture and lysimeter experiments were used for validation. Pakistan Agricultural Research Council (PARC) measured actual ET at Peshawar, Bhalwal, Faisalabad, Bhakkar, MianChannu, and Tandojam representing upper, middle and lower parts of the basin [*PARC*, 1982]. The ET results of PARC are for the years 1975–80 following an internationally funded study. Data collection discontinued when the project ended, yet it seems to be one of the most basic databases in Pakistan. More recent field measurement study was conducted by *Ahmad* [2002] at the Soil Salinity Research Institute, Pindi Bhattian (31°52′34.2″N, 73°20′50.2″E) and Ayub Agricultural Research Institute, Faisalabad (31°23′26.2″N, 73°02′49.8″E). As part of a field investigation program during 2000 and 2001, he measured actual ET in rice/wheat and cotton/wheat systems by a temporarily installed Bowen ratio energy balance system.

[31] ETLook estimates were also checked against previously conducted remote sensing and modeling studies. The ET estimates provided by *Bastiaanssen et al.* [1999] for the Sirsa irrigation circle in India were checked. Other studies [e.g., *Shakoor et al.*, 2006; *Sarwar and Bill*, 2007; *Ahmad et al.*, 2009; *Shakir et al.*, 2010] determined ET in selected areas within the basin for different years. Previous studies were synthesized and used to compare with ETLook estimates. The coefficient of determination (R^2), Root Mean Square Error (RMSE) and Relative Error (RE) were calculated to estimate the difference of the ETLook estimates with the previous studies.

3.5. Sensitivity and Uncertainty Analysis

[32] A sensitivity analysis was performed to check the contribution of selected main input parameters to the output results. The sensitivity of ET was tested for a number of input parameters, i.e., θ_{AMSRE}, NDVI, $r_{s,\min}$, r_{soil} and θ_{sat}. Annual mean climatic conditions were assumed for the analysis. One factor at a time methodology was adopted to check the variance in the outputs due to input variability [e.g., *Pitman*, 1994]. The analysis was conducted on two representative land uses, i.e., "bare soil" and "irrigated rice-wheat rotation" at locations 71°22′54.123″E, 28°38′50.042″N and 75°23′53.59″E, 30°40′37.719″N, respectively. Randomly generated uniform distribution of AMSR-E based soil moisture values ($n = 1000$) were used while keeping other parameters constant to check the variations in E, T and ET. The analysis was performed using representative NDVI values of 0.05 for bare soil and 0.67 for irrigated land use. A complete sensitivity analysis representing the change in the response variable caused by a unit change of an explanatory variable, while holding the rest of parameters constant, was performed. A Sensitivity Coefficient (SC = $\Delta_{\mathrm{out}}/\Delta_{\mathrm{in}}$) was then calculated for each input parameter as described by *Gu and Li.* [2002]. The sensitivity coefficient was normalized by the mean values representing the range of each pair of output and input variable. This normalized sensitivity coefficient is called Sensitivity Index (SI) and can be positive or negative. SI makes it feasible to compare the results of different input parameters. A higher absolute value indicates higher sensitivity. A negative SI indicates an inverse relationship between input parameter and response variable. SI can be represented as:

$$SI = (M_{\mathrm{in}}/M_{\mathrm{out}})(\Delta_{\mathrm{out}}/\Delta_{\mathrm{in}}), \tag{20}$$

where M_{in} and M_{out} are the mean values of the input and output range, respectively.

[33] In addition, a stochastic uncertainty analysis was performed. A Monte Carlo simulation experiment using 1000 pairs of randomly generated input parameters was performed to investigate the model uncertainty. The values of the sensitive parameters were varied, while other climatic variables were kept constant.

4. Results

4.1. Surface Energy Balance

[34] The temporal variation of each component of the surface energy balance of the Indus Basin for the hydrological year 2007 is presented in Figure 2. The values represent the spatial averages for the whole Indus Basin. The average values attained by the surface energy fluxes with their standard deviations (SD) are provided in Table 1. A high variability from the mean is observed for the year, especially for net shortwave radiation ($R^{\downarrow}$), net radiation (R_n) and sensible heat flux (H). The large variation in climate during summer and winter is the probable cause of the high SD.

[35] R_n is the dominant source of energy for land surface processes. The annual average value for R_n was 112.3 Wm^{-2} with a standard deviation of 46.7 Wm^{-2}. The lower R_n values (<80 Wm^{-2}) prevailed during the winter season (DOY 305–361 and 1–65). This low R_n is probably due to

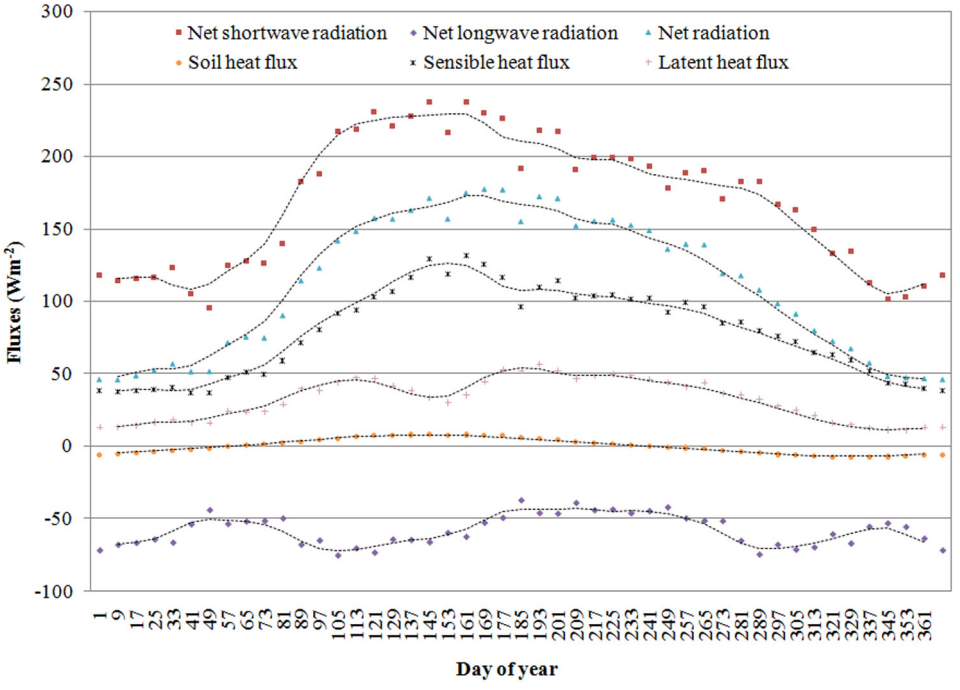

Figure 2. Temporal variation of components of the surface energy equation during 2007 in the entire Indus Basin (116.2 mha). The dashed lines represent 24 days moving average values.

the lower net shortwave radiation. After DOY 66, the R_n continuously increased to a maximum of 177.4 Wm^{-2} for an 8 day period (DOY 161). In the summer season the maximum R_n (>150 Wm^{-2}) was observed during DOY 113–225 while the average was 163.5 Wm^{-2}. For the same period, R_n values fluctuated considerably with sudden depressions during DOY 145–225, corresponding to the monsoon season with clouds. Afterward, the net radiation decreased gradually and reached its minimum values again in winter.

[36] The dry arid environment of the Indus Basin (annual rainfall is 383 mm) causes the net radiation to dissipate mainly into sensible heat flux (H). H followed the same temporal pattern as that of the net radiation and the daily mean value varied between a minimum of 37.2 and maximum of 131.6 Wm^{-2}. The average annual value for a 24 h period of H was 79.5 Wm^{-2}. When the soil is moist, a significant part of the energy is dissipated into evaporation. λE showed two peaks during its annual cycle (Figure 2).

Table 1. Minimum, Maximum, and Average Values of Surface Energy Fluxes in the Indus Basin Attained During the Year 2007[a]

Fluxes	Minimum	Maximum	Mean	SD
Net shortwave radiation (Wm^{-2})	95.70	237.50	170.10	45.10
Net longwave radiation (Wm^{-2})	–75.60	–36.90	–57.80	10.80
Net radiation (Wm^{-2})	46.20	177.40	112.30	46.70
Soil heat flux (Wm^{-2})	–7.10	8.10	0.34	5.20
Sensible heat flux (Wm^{-2})	37.20	131.60	79.50	29.80
Latent heat flux (Wm^{-2})	10.90	57.00	32.40	14.30
Evapotranspiration (mm d^{-1})	0.39	2.10	1.20	0.50
Evaporative fraction (=)	0.19	0.36	0.28	0.05

[a]The entire basin is covered and the values represent average flux densities for periods of eight days including daytime and nighttime.

The seasonal peaks for the entire Indus Basin correspond to the two agricultural seasons, once in *rabi* and once in *kharif*. The λE varied in the range from 10.9 (during winter with more cloud covers and lower temperatures) to 57 Wm^{-2} (during the periods of more canopy cover and higher temperature), with an annual average of 32.4 Wm^{-2}. The average λE for the entire Indus Basin coincided with an ET of 1.2 mm d^{-1}, but large variability among LULC classes occurred. The basin-wide evaporative fraction (Λ) is calculated as 0.28, equivalent to a Bowen ratio of 2.5. Hence, the amount of sensible heat released into the atmosphere is 2.5 times more than for water vapor, if both are expressed in energy terms.

[37] Soil heat flux (G) is normally ignored when seasonal averages are considered because of its small scale. However, G can account for a significant portion (3 – 5%) of the total energy during summer (DOY 113–171) indicating that G is transferred from shallow to deep soil while for the rest of the year, the reverse process occurs.

4.2. Actual Evapotranspiration Estimates

[38] The total transpiration and evaporation in the basin was estimated at 233 km^3 yr^{-1} and 263 km^3 yr^{-1}, respectively. The major portion of water was consumed as nonbeneficial evaporation (E), mainly from water-logged soils, dry soils and open water bodies. High annual ET values occurred on the alluvial plains as depicted in Figure 3. Irrigated agriculture is the major land use class (22.6%) in the basin and is a major consumer of water. It accounts for the annual ET rates of between 700 and 1200 mm and represents the middle part of the frequency distribution in Figure 4. The highest values (1200–1550 mm yr^{-1}) were found in the tail end of the basin: in particular in the right bank of the

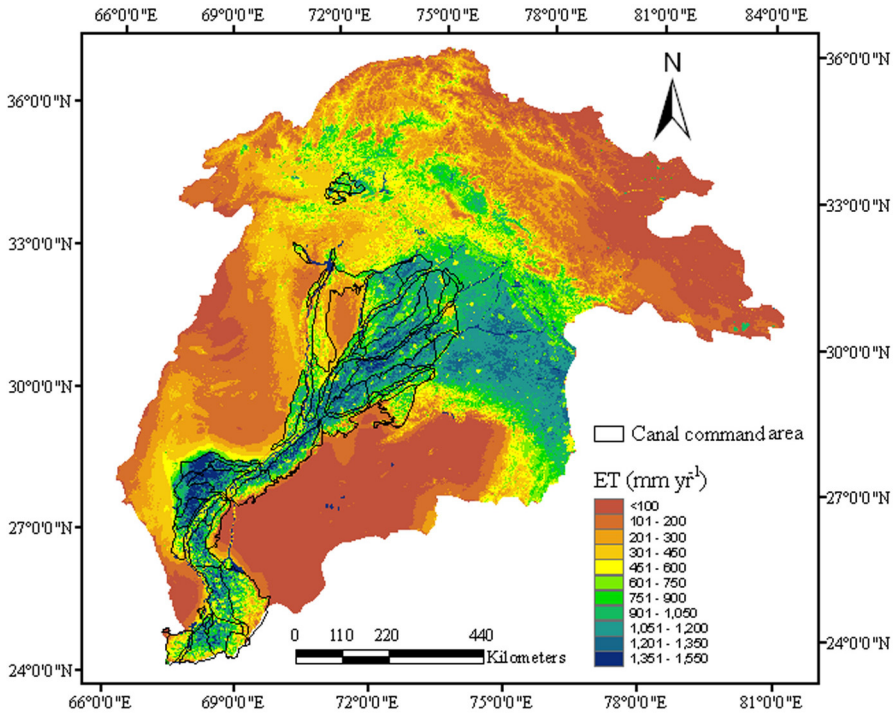

Figure 3. ETLook estimated cumulative actual evapotranspiration for the hydrological year 2007 (January to December). The canal command areas for irrigated cropland are superimposed on the ET map.

Indus River, and southern parts toward the Indian Ocean, in the Sindh Province of Pakistan. Water-logged soils, rice paddies with shallow phreatic surfaces, and flooded areas normally occur in these parts of the basin, especially during *kharif*. Besides higher soil water content, factors such as higher solar radiation, higher air temperatures, more rainfall, and cultivation of higher consumptive use crops are the reasons for the higher ET.

[39] Figure 4 provides the frequency distribution of annual ET. The average ET for all land use classes was

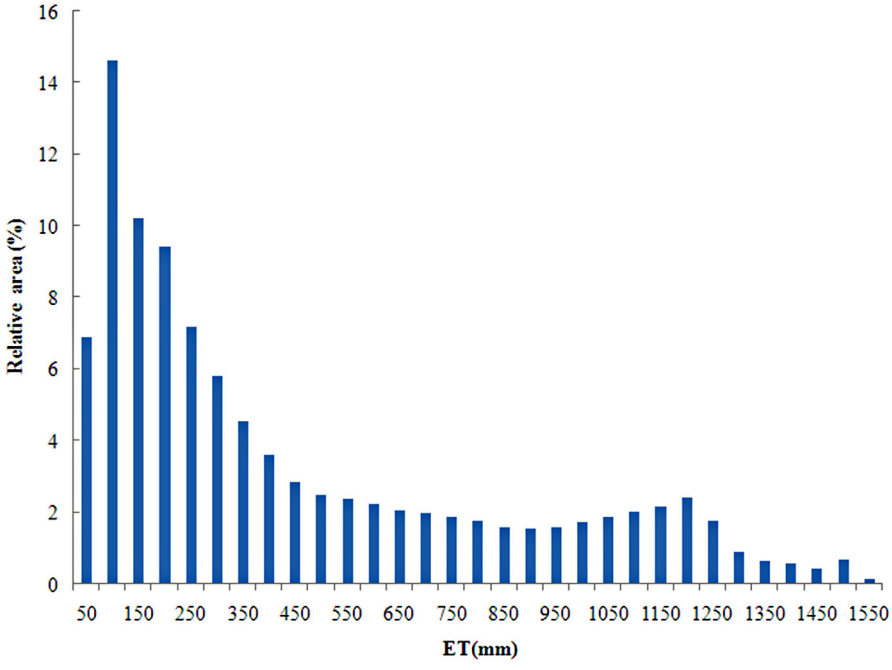

Figure 4. Frequency distribution of the ETLook estimated annual ET in the Indus Basin at spatial resolution of 1 km × 1km for 2007.

426 mm yr^{-1} during 2007. The 2% lowest value was 60 mm yr^{-1} and the 2% highest value was 1550 mm yr^{-1}.

[40] A sensitivity analysis was performed to understand the role of topsoil moisture data in the ET estimation procedure. The results are provided in Figures 5a and 5b. Two land use classes and the average climatological condition of the year were used.

[41] The curves in the Figures 5a and 5b display the response of model outputs (E and T) to variation in surface soil moisture. It is evident from the figure that the ET responds to surface soil moisture variability. Bare soil shows a fast response in E to surface soil moisture, while T remains negligibly small by absence of leaves (NDVI = 0.05). E is the dominant flux in the overall ET process of bare soil. The response is curvilinear with the highest sensitivity occurring between 0.05 and 0.25 cm^3 cm^{-3}. The effects are lower when $\theta > 0.25$ cm^3 cm^{-3} prevails. The parameter r_{soil} and the nonlinearity of equation (11) is one reason for this result. Another explanation is the nonlinear relationship between the resistance and the latent heat fluxes that generally exists (not shown in this paper). The combined effect yields the S-type curve that is portrayed in Figure 5a, and to a lesser extent in Figure 5b.

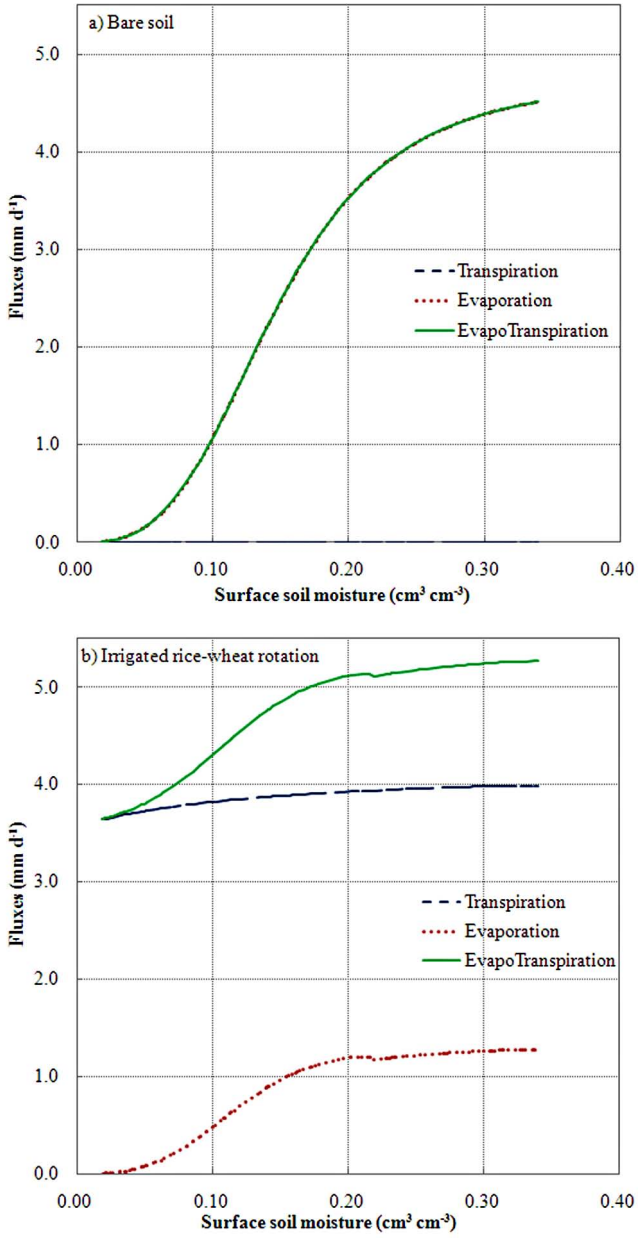

Figure 5. The response of evaporation, transpiration and evapotranspiration rates to surface soil moisture ($n = 100$) for two representative land uses (a) Bare soil (71°22′54.123″E, 28°38′50.042″N) and (b) Irrigated rice-wheat rotation (75°23′53.59″E, 30°40′37.719″N). NDVI values of 0.05 and 0.67 were selected for bare soil and full grown irrigated rice-wheat land use, respectively.

[42] Figure 5b reveals that, in closed canopies, T dominates E. The net radiation is absorbed partially by the canopy, and the bare soil surface receives less energy for evaporation. At an NDVI of 0.67, E increases with increasing topsoil moisture, up to 0.18 cm^3 cm^{-3}. Apparently there is always soil evaporation in rice-wheat rotation systems, which is confirmed by many other agrohydrological studies [e.g., *Ahmad et al.*, 2002; *Sarwar and Bastiaanssen*, 2001]. Canopy transpiration depends entirely upon root zone soil moisture rather than on the surface soil moisture. This is correct as crop can transpire intensely while the topsoil is dry. This is in fact promoted by introducing drip irrigation systems. Therefore, T shows less sensitivity to surface soil moisture. The same can be concluded on the total ET response to surface soil moisture changes.

[43] The effect of other input parameters on ET is summarized in Table 2. The lower and higher ranges of model input parameters are given, together with ET estimates for the average climate in the Indus Basin. The values of the input parameters were changed with specific increments. The sensitivity index (SI) was determined and the parameters were ranked based on the absolute values. The surface soil moisture appears to be the most important parameter for describing ET variability, with ET values ranging from 2.3 to 6.3 mm d^{-1}, followed by the coefficient c in r_{soil} with a range of 2.5 to 6.2 mm d^{-1}. The measurements of AMSR-E are thus essential for achieving proper ET modeling results, and form the key input parameter of ETLook as was suggested in the introduction.

[44] Model parameter sensitivity was investigated using a Monte Carlo simulation experiment with 1000 pairs of randomly generated input parameters. Based on this experiment the mean ET for "irrigated rice-wheat rotation" was 3.2 mm d^{-1} with an SD of 1.7 mm. The standard error for this distribution was 0.05 mm. A 95% confidence interval was used to determine the 2.5th and 97.5th percentiles, which ranged between 3.1 and 3.3 mm d^{-1}. This level of uncertainty reflects that the model generates results with a potential error of 3.4%.

4.3. Validation

4.3.1. Field Measurements

[45] Several field methods to measure ET fluxes can be used to validate the results. AsiaFlux has erected flux towers in China and India, but not in Pakistan [*Mizoguchi et al.*, 2009]. Therefore, to evaluate performance, ET estimates by ETLook were compared with the measured values given by *PARC* [1982] and *Ahmad* [2002] for 1975–1980

Table 2. Sensitivity of Estimates of ET to Model Parameter Values for Irrigated Rice-Wheat Land Use[a]

Parameter	Input Value					Resulted ET (mm)						
	Min	Base[b]	Max	Δ_{in}	M_{in}	Min	Base	Max	Δ_{out}	M_{out}	SC	SI
θ_{AMSRE} ($cm^3\ cm^{-3}$)	0.05	0.15	0.35	0.30	0.2	2.3	5.1	6.3	4.0	4.3	13.3	0.62
r_{soil}, c ($s\ m^{-1}$)	−10.0	−3.0	5.0	15	7.5	2.5	5.1	6.2	3.7	4.3	0.23	0.40
$r_{s,min}$ ($s\ m^{-1}$)	40.0	80.0	500	460	270	5.6	5.1	3.4	−2.2	4.5	−0.005	−0.3
NDVI (-)	0.05	0.45	0.67	0.62	0.36	3.9	5.1	5.9	2.0	4.9	3.2	0.24
r_{soil}, b ($s\ m^{-1}$)	10.0	30.0	70.0	60	40	5.8	5.1	4.3	−1.5	5.1	−0.025	−0.2

[a]The last column depicts the sensitivity in terms of slope. Δ is change, and *M* is mean.
[b]Definition of fixed reference values during sensitivity test.

and 2000–2001, respectively (onward referred to as "measured" values). Figure 6 shows the results of irrigated crops.

[46] The correlations were good with an R^2 of 0.70, and an RMSE of 163 mm (0.45 mm d^{-1}). The RE between ETLook and measured ET values ranged from –1.9% to –28% with an average of –11.5%. The negative RE means ET figures from ETLook were lower than the field measurements. The regression line fitted through the origin has a slope of 0.89. This implies that ETLook estimates for 2007 were 11% lower than ET from previous studies. This difference of 11% is acceptable, considering the climatic differences between the years, the scale difference between in situ measurements, and the 1 km remote sensing pixel size, as well as the uncertainty embedded in field measurements.

[47] Figure 7 shows the comparison of annual and seasonal ET from ETLook, from previous remote sensing and modeling studies (year 1995–96, 2001–02), and from other models (year 2000, 1999–2006) (onward referred to as "modeled" values). There is a reasonably good agreement between ETLook estimates and modeled values at annual scale, with an R^2 of 0.76 and an RMSE of 108 mm yr^{-1} (or 0.29 mm d^{-1}). The values for the *rabi* season are reasonable (R^2 of 0.60 and RMSE of 47.9 mm). However, the *kharif* season shows a relatively low R^2 (0.54) and a high RMSE of 70.7 mm (or 0.39 mm d^{-1}). Note that there is no bias toward the lower or higher end of the ET data, and that the average slope is 1.05. Since Figure 6 suggests an underestimation of ET, and Figure 7 an overestimation, we believe that the ETLook estimates of ET are within a plausible and acceptable range for this type of vast basins with scarce data.

[48] ETLook has also been validated in regions other than the Indus, e.g., Australia and China. Some of these unpublished results are presented as a demonstration of the model performance under different climates and landscapes of ETLook. The National Water Commission of the Australian Government has provided Australian Water Resources (AWR) data for the year 2005.The water use data of eight states and 23 jurisdictional areas are publically available through http://www.water.gov.au/. The ET is computed as the difference between rainfall and runoff; storage changes and groundwater are not considered. ET values from the water balance were compared against ETLook (Figure 8). Considering that the annual values were averaged over a large area, correlation was reasonable with an R^2 of 0.70 and an RMSE of 112 mm (0.31 mm d^{-1}). The RE between the ETLook and AWR ET values ranged from –40% to 36% with an average of –2.8%.

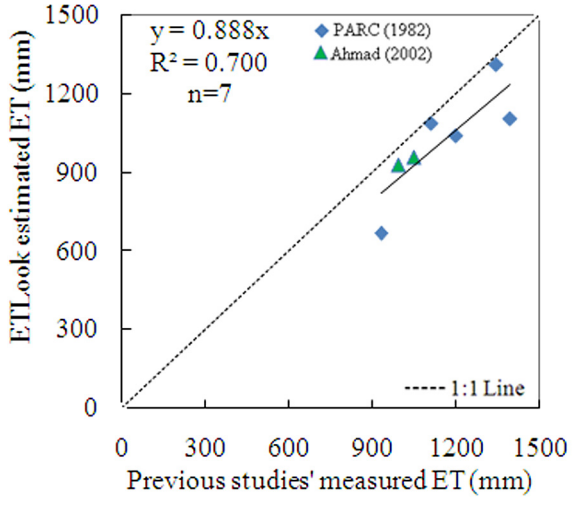

Figure 6. A comparison of evapotranspiration in rice-wheat rotation measured by previous studies, and those estimated by ETLook for 2007 in the Indus Basin.

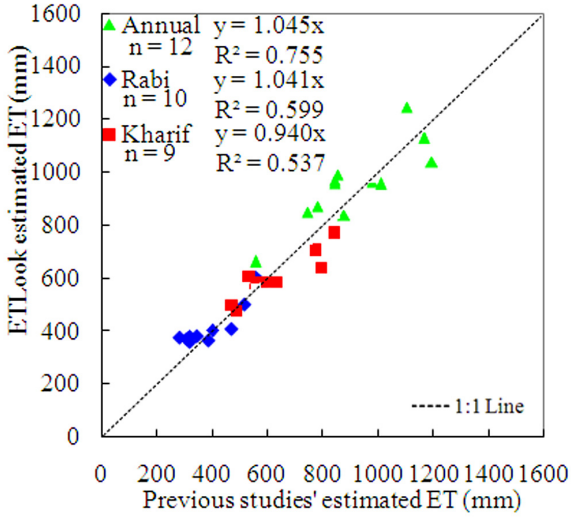

Figure 7. Comparison of evapotranspiration modeled/estimated by previous studies conducted during the years 1995–1996 [*Bastiaanssen et al.*, 1999], 2000 [*Sarwar and Bill*, 2007], 2001–2002 [*Ahmad et al.*, 2009; *Shakoor et al.*, 2006] and 1999–2006 [*Shakir et al.*, 2010] and ET estimated by ETLook for 2007 in the Indus Basin.

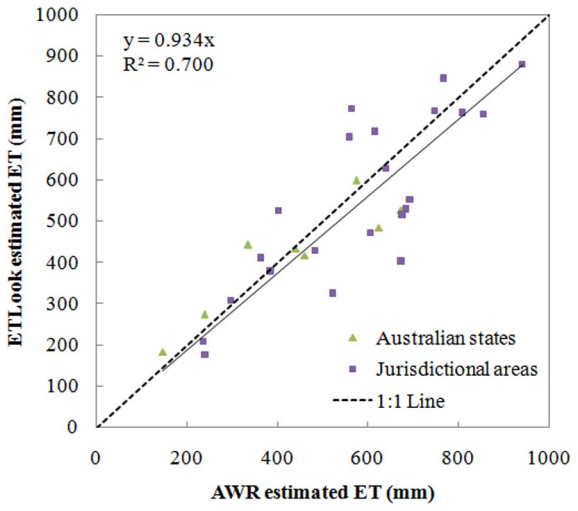

Figure 8. Comparison of evapotranspiration estimated by ETLook and estimates provided by Australian water commission for the year 2005.

[49] In China, ETLook estimated latent heat flux in the year 2009 was compared with flux tower measurements obtained from the eddy covariance flux measurement station at Heibei, Qinghai, China (37°36′N, 101°20′E) (Figure 9). Annual values correlated well with an R^2 of 0.92 and an RMSE of 11 mm (0.04 mm d^{-1}). The RE of 9.5% between the two datasets shows that the ETLook estimated ET falls within the range of the ground measurements considering the mismatch of scales between 1 km ETLook pixel estimates and ground measurements (flux tower).

4.3.2. Water Balance

[50] A map depicting differences in rainfall and evapotranspiration (R–ET) was prepared using TRMM rainfall data, calibrated by *Cheema and Bastiaanssen* [2012], and the ET results from this study (Figure 10). It shows areas with net water production (R > ET) and areas with net water consumption (ET > R). This indicates the value of spatial data to describe hydrological processes and withdrawals. The pixels that produce water (R > ET) are discharge areas responsible for streamflow and groundwater recharge. These areas are in the upstream parts of the basin, and are the source of the rivers Indus, Jhelum and Sutlej that feed the large reservoirs Tarbela, Mangla and Bhakra, respectively. Areas with sparse vegetation and low ET also have higher rainfall than ET and are water producing areas. Large parts of the Tibetian Plateau comprise such areas. The Rajasthan Desert between India and Pakistan also exhibits positive values of R–ET, which suggests groundwater recharge.

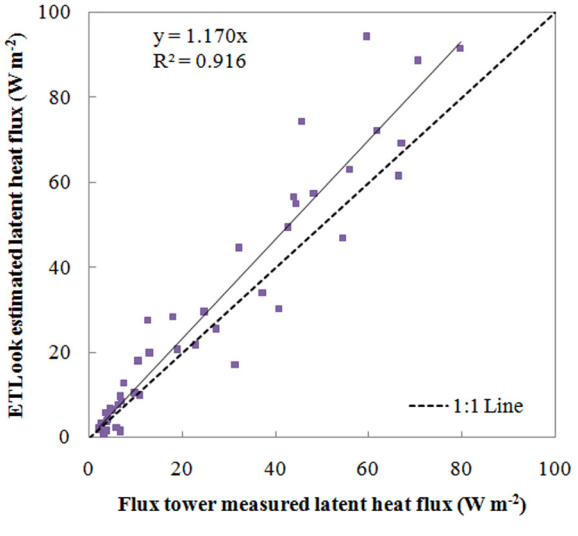

Figure 9. Comparison of latent heat flux estimated by ETLook and measured by flux tower at Heibei, Qinghai, China (37°36′N, 101°20′E) for the year 2009. Each point represents 8-day average value.

[51] Net water consumption areas are generally the irrigated areas, lakes and reservoirs. Irrigation increases crop ET far beyond the level of rainfed crops. In the Indus Basin, 30.3% of the total land area is composed of net consumer areas, and 22.6% (26.02 mha) is irrigated land. The mountain valleys are net water consumers; the valleys receive both seepage water through the groundwater system and surface water from the higher elevated mountains, which generally results in shallow water table areas in the vicinity of streams.

[52] The water balance of the irrigated areas covering 26.02 mha was computed to validate ET results on a large scale (Table 3). Total annual groundwater abstraction in Pakistan's part of the Indus Basin is given by *Qureshi et al.* [2010] as 51 km^3. *Chadha* [2008] estimated that for the Indian part of the Indus Basin 18.5 km^3 is being abstracted from the groundwater system. This totals to 69.5 km^3 yr^{-1}. The surface water releases into the main canals add up to 122 and 36 km^3 yr^{-1} in Pakistan and India, respectively. These data on releases from Tarbela, Mangla, Chashma, Thein, Pong and Bhakra reservoirs, as well as flows into the main irrigation canals were obtained from Punjab Irrigation Department and Indus Water Commission, Pakistan. If we assume a conveyance efficiency of 80% that is locally checked and verified [*Habib*, 2004; *Jeevandas et al.*, 2008], then 126.4 km^3 yr^{-1} will arrive at the farm gate through the network of canals. Adding the 69.5 km^3 [*Chadha*, 2008; *Qureshi et al.*, 2010] of groundwater from locally operating tubewells the total amount of water used is about 196 km^3. If we take an on-farm irrigation efficiency of 80% to describe losses of water that is not properly stored in the root zone, the total ET from irrigation will be 156.8 km^3 yr^{-1}. Note that a regional scale on-farm efficiency for the total irrigation system includes recycling of nonconsumed irrigation water [*Perry*, 2007]. A total irrigation efficiency of 64% (0.8 × 0.8) for one contiguously irrigated alluvial plain can be considered realistic [*Habib*, 2004; *Seckler et al.*, 1999]. It can however also be 60% or 70%. The rainfall over the irrigated area is 117 km^3 yr^{-1}. The net rainfall infiltrated into the soil—after runoff and percolation losses—and available for uptake by roots is 94 km^3 yr^{-1} (assuming 80% efficiency). The total ET for the irrigated land on the basis of water balance is 94 + 156.8 = 250.8 km^3 yr^{-1}, or 964 mm yr^{-1}. ETLook results provided an estimate on the basis of the energy balance as being 254 km^3 yr^{-1}, or 974 mm yr^{-1}. Without any further data at

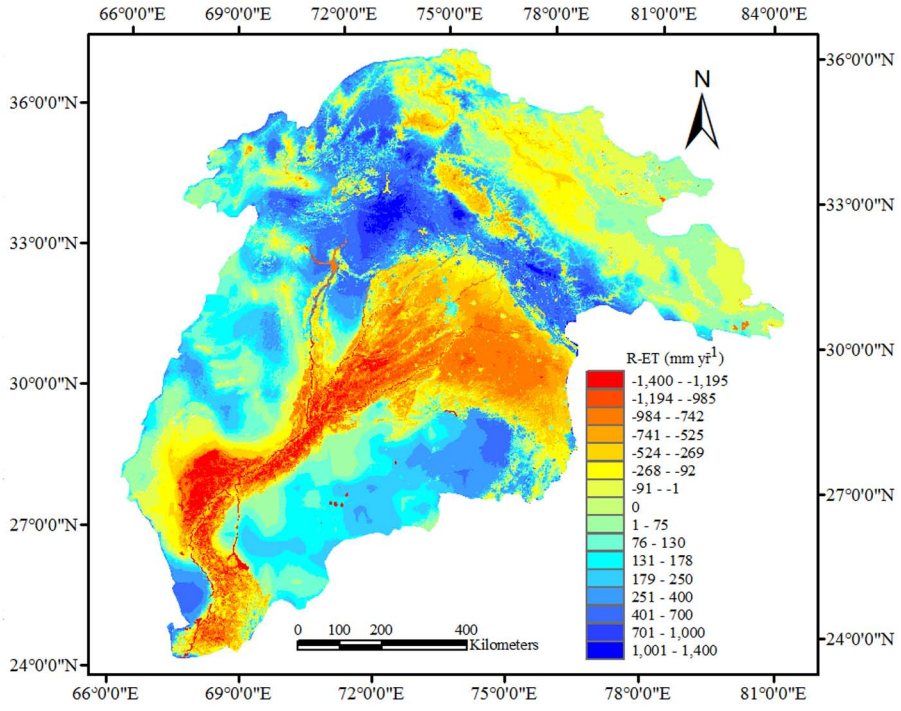

Figure 10. Rainfall-Evapotranspiration (R–ET) difference map of the Indus Basin for the hydrological year 2007.

hand, we conclude that the results are congruent and within acceptable ranges that are usually related to water balances of irrigated areas.

5. Limitations

[53] The power of having access to daily soil moisture data from passive microwave measurements onboard satellites is at the same time a limitation by the low resolution of AMSR-E surface soil moisture pixels (25 km). Several methods exist to deal with the downscaling of soil moisture, but the best method that is doable under a wide range of conditions still needs to be found. More sophisticated solutions on downscaling can be gleaned from topographic information (e.g., height above drain, distance to drain, accumulated upstream drainage area) and soil properties (infiltration capacity, water holding capacity, drainage capacity). It is expected that satellites with synthetic aperture radar will provide high-resolution soil moisture values in an operational context in the near future, in addition to the thermal data. The analytical relationships between topsoil and subsoil moisture need improvement and more testing under different environmental conditions. For this reason we refer to this version of ETLook as 1.0. An improved parameterization of S_e^{sub} using various combinations of climate, soil types, drainage conditions and LAI is under development. A more complex solution for equation (2) will however not necessarily improve the performance of ETLook.

[54] The soil moisture estimated by AMSR-E does have limitation to use, but availability of new data sources on soil moisture will improve the situation. New sophisticated satellites e.g., Soil Moisture and Ocean Salinity (SMOS) and Advanced SCATterometer (ASCAT) can be best alternatives of AMSR-E. With the discontinuity of AMSR-E and SMOS data, we believe that the ASCAT data is a good replacement of AMSR-E, and it provides an operational data flow of day-to-day variability of moisture conditions.

[55] This analysis was conducted for a one year cycle only, to raise confidence in using the first version of ETLook algorithm (ETlook 1.0). Future analysis with longer time series is recommended, since shorter time series may be of low significance. Despite the limitations mentioned, the current paper has demonstrated that the ET results show potential for determining water depletion in ungauged basins, and that the results are congruent with the other sources of ET data.

6. Summary and Conclusions

[56] The first requirement for an operational ET monitoring system is that the satellite data must be available at all

Table 3. Water Balance for the Irrigated Areas in the Indus Basin During the Hydrological Year 2007

		Irrigation (IRR)				Evapotranspiration (ET)			
	Annual Rainfall R	From Surface Water	At Farm Gate	From Ground Water	Total (Column 4 + 5)	IRR	R	Total	ET_{ETLook}
km^3	117	158	126.4	69.5	196	156.8	94	250.8	254
mm	451	607	486	267	753	603	361	964	974

times. Microwave satellite data are operationally provided—even under all weather conditions—and their growing number of standard databases form an attractive source for developing ET models. ETLook can assess the spatial and temporal (daily, 8-day, or monthly) patterns of the surface energy balance and actual evapotranspiration. Computing E and T separately, on the basis of the energy balance, has the advantage that complex transient moisture flow computations in the unsaturated topsoil can be circumvented. The novelty of this paper is a doable computational method for nonbeneficial E and beneficial T that can be applied under conditions of persistent overcast skies, and in data scarce environments. The sensitivity analysis revealed that the surface soil moisture is the most important parameter for describing ET variability. Variability of surface soil moisture revealed that the ET values for rice-wheat rotation system on an average day ranged between 2.3 to 6.3 mm d^{-1}, followed by the coefficient c of soil resistance, with a range of 2.5 to 6.2 mm d^{-1}.

[57] Good agreement was attained between ETLook and previously conducted field measurements and remote sensing studies. R^2 varied between 0.70 and 0.76 at annual time scale (RMSE: 0.45 and 0.29 mm d^{-1}, respectively). Tests in Australia and China provided similar agreements based on watershed measurements. The water balance of 26.02 mha of irrigated land is congruent and matches generic data on surface water and groundwater supply. There are discrepancies in timescales shorter than a year. However, no bias was evident toward the lower or higher end of the ET values. The observed errors could be due to the meteorological differences between the years of study. The determination of wind speed and air humidity needs more attention in future studies. Better quality soil maps will also improve the quality of the ET results.

[58] The average value for latent heat flux in the Indus Basin is 32 Wm^{-2}, which corresponds with an ET of 1.2 mm d^{-1} (426 ± 14.5 mm yr^{-1}). The average value for rainfall is 383 mm yr^{-1}. Over-exploitation and negative storage changes of water occur at the basin scale (ET > R). The negative change in storage can be ascribed to reduced volumes of water stored in reservoirs and aquifers. Retirement of glaciers also contribute to water storage changes.

[59] **Acknowledgments.** The authors are thankful to the Higher Education Commission (HEC) of Pakistan for providing funds to carry out this research. Thanks also go to the Pakistan Meteorological Department, Punjab Irrigation Department, and Indus Water Commission, in Pakistan, for providing required data. Peter Droogers of FutureWater, kindly provided the soil physical properties required for the soil moisture downscaling. The authors are also thankful to Ms. Annemarie Klaasse (Water Watch) for providing necessary support in collecting satellite data. We thank the anonymous reviewers for their helpful comments to improve the quality of the manuscript.

References

Ahmad, M. D. (2002), Estimation of net groundwater use in irrigated river basins using geo-information techniques: A case study in Rechna Doab, Pakistan, Ph.D. dissertation, 143 pp, Wageningen, Netherlands.

Ahmad, M. D., W. G. M. Bastiaanssen, and R. A. Feddes (2002), Sustainable use of groundwater for irrigation: A numerical analysis of the subsoil water fluxes, *Irrig. Drain.*, *51*(3), 227–241.

Ahmad, M. D., W. Bastiaanssen, and R. Feddes (2005), A new technique to estimate net groundwater use across large irrigated areas by combining remote sensing and water balance approaches, Rechna Doab, Pakistan, *Hydrogeol. J.*, *13*(5), 653–664.

Ahmad, M. D., H. Turral, and A. Nazeer (2009), Diagnosing irrigation performance and water productivity through satellite remote sensing and secondary data in a large irrigation system of Pakistan, *Agric. Water Manage.*, *96*, 551–564.

Allen, R. G., L. S. Pereira, D. Raes, and M. Smith (1998), Crop evapotranspiration-guidelines for computing crop water requirements, *FAO Irrig. Drain. Pap. 56*, FAO, Rome, Italy.

Allen, R. G., et al. (2006), A recommendation on standardized surface resistance for hourly calculation of reference ETo by the FAO56 Penman-Monteith method, *Agric. Water Manage.*, *81*(1–2), 1–22.

Allen, R. G., M. Tasumi, and R. Trezza (2007), Satellite-based energy balance for mapping evapotranspiration with internalized calibration (METRIC)—Model, *J. Irrig. Drain. Eng.*, *133*(4), 380–394.

Allen, R. G., J. Hendrickx, W. G. M. Bastiaanssen, J. Kjaersgaard, A. Irmak, and J. Huntington (2010), Status and continuing challenges in operational remote sensing of ET, in *ASABE 5th National Decennial Irrigation Conference Proceedings*, edited, Phoenix Convention Center, Phoenix, Ariz.

Allen, R., A. Irmak, R. Trezza, J. M. H. Hendrickx, W. G. M. Bastiaanssen, and J. Kjaersgaard (2011), Satellite-based ET estimation in agriculture using SEBAL and METRIC, *Hydrol. Processes*, *25*, 4011–4027.

American Society of Civil Engineers (1996), Hydrology Handbook, American Society of Civil Engineers Task Committee on Hydrology Handbook, *Am. Soc. Civ. Eng. Publ. 28*, pp. 784.

Anderson, M. C., J. M. Norman, J. R. Mecikalski, J. A. Otkin, and W. P. Kustas (2007), A climatological study of evapotranspiration and moisture stress across the continental United States based on thermal remote sensing: 2. Surface moisture climatology, *J. Geophys. Res.*, *112*, D11112, doi:10.1029/2006JD007507.

Angstrom, A. (1924), Solar and terrestrial radiation, *Q. J. R. Meteorol. Soc.*, *50*(210), 121–126.

Barnard, J. C., and C. N. Long (2004), A simple empirical equation to calculate cloud optical thickness using shortwave broadband measurements, *J. Appl. Meteorol.*, *43*, 1057–1066.

Bastiaanssen, W. G. M., and K. Bandara (2001), Evaporative depletion assessments for irrigated watersheds in Sri Lanka, *Irrig. Sci.*, *21*(1), 1–15.

Bastiaanssen, W. G. M., T. Van der Wal, and T. N. M. Visser (1996), Diagnosis of regional evaporation by remote sensing to support irrigation performance assessment, *Irrig. Drain. Syst.*, *10*(1), 1–23.

Bastiaanssen, W. G. M., D. J. Molden, S. Thiruvengadachari, A. A. M. F. R. Smit, L. Mutuwatte, and G. Jayasinghe (1999), *Remote Sensing and Hydrologic Models for Performance Assessment in Sirsa Irrigation Circle, India*, Int. Water Manage. Instit., Colombo, Sri Lanka.

Bastiaanssen, W. G. M., H. Pelgrum, R. W. O. Soppe, R. G. Allen, B. P. Thoreson, and A. H. Teixeira (2008), Thermal-infrared technology for local and regional scale irrigation analyses in horticultural systems, *Acta Hortic.*, *792*, 33–46.

Braden, H. (1985), Ein energiehaushalts und verdunstungsmodell fur Wasser und Stoffhaushaltsuntersuchungen landwirtschaftlich genutzer einzugsgebiete, *Mittelungen Dtsch. Bodenkundliche Geselschaft*, *42*, 294–299.

Brutsaert, W. H. (1982), *Evaporation Into the Atmosphere: Theory, History, and Applications*, Reidel Publ., Dordrecht, Netherlands.

Burke, E. J., W. J. Shuttleworth, and A. N. French (2001), Using vegetation indices for soil-moisture retrievals from passive microwave radiometry, *Hydrol. Earth Syst. Sci.*, *5*(4), 671–678.

Calcagno, G., G. Mendicino, G. Monacelli, A. Senatore, and P. Versace (2007), Distributed estimation of actual evapotranspiration through remote sensing techniques, in *Methods and Tools for Drought Analysis and Management*, edited by G. Rossi et al., pp. 125–147, Springer, Netherlands.

Camillo, P. J., and R. J. Gurney (1986), A resistance parameter for bare-soil evaporation models, *Soil Sci.*, *141*(2), 95–105.

Carlson, T. N., and D. A. Ripley (1997), On the relation between NDVI, fractional vegetation cover, and leaf area index, *Remote Sensing Environ.*, *62*(3), 241–252.

Chadha, D. K. (2008), Development, management and impact of climate change on transboundary aquifers of Indus Basin, paper presented at *4th International Symposium on Transboundary Water Management*, Aristotle Univ. of Thessaloniki, Thessaloniki, Greece, 15–18 Oct.

Cheema, M. J. M., and W. G. M. Bastiaanssen (2010), Land use and land cover classification in the irrigated Indus Basin using growth phenology information from satellite data to support water management analysis, *Agric. Water Manage.*, *97*, 1541–1552.

Cheema, M. J. M., and W. G. M. Bastiaanssen (2012), Local calibration of remotely sensed rainfall from the TRMM satellite for different periods

and spatial scales in the Indus Basin, *Int. J. Remote Sensing*, *33*(8), 2603–2627.

Cheema, M. J. M., W. G. M. Bastiaanssen, and M. M. Rutten (2011), Validation of surface soil moisture from AMSR-E using auxiliary spatial data in the transboundary Indus Basin, *J. Hydrol.*, *405*(1–2), 137–149.

Choudhury, B. J., R. J. Reginato, and S. B. Idso (1986), An analysis of infrared temperature observations over wheat and calculation of latent heat flux, *Agric. For. Meteorol.*, *37*, 75–88.

Clapp, R. B., and G. M. Hornberger (1978), Empirical equations for some soil hydraulic properties, *Water Resour. Res.*, *14*(4), 601–604.

Courault, D., B. Seguin, and A. Olioso (2005), Review on estimation of evapotranspiration from remote sensing data: From empirical to numerical modeling approaches, *Irrig. Drain. Syst.*, *19*, 223–249.

Curran, P. J., and M. D. Steven (1983), Multispectral remote sensing for the estimation of green leaf area index and discussion, *Philos. Trans. R. Soc. London Ser. A*, *309*(1508), 257–270.

de Fraiture, C., and D. Wichelns (2010), Satisfying future water demands for agriculture, *Agric. Water Manage.*, *97*(4), 502–511.

Dolman, A. J. (1993), A multiple-source land surface energy balance model for use in general circulation models, *Agric. For. Meteorol.*, *65*(1–2), 21–45.

Droogers, P., W. W. Immerzeel, and I. J. Lorite (2010), Estimating actual irrigation application by remotely sensed evapotranspiration observations, *Agric. Water Manage.*, *97*, 1351–1359.

Elhaddad, A., and L. A. Garcia (2008), Surface energy balance-based model for estimating evapotranspiration taking into account spatial variability in weather, *J. Irrig. Drain. Eng. ASCE*, *134*(6), 681–689.

Fily, M., J.-P. Dedieu, and S. Surdyk (1995), A SAR image study of a snow-covered area in the French Alps, *Remote Sensing Environ.*, *51*(2), 253–262.

Food and Agriculture Organization (FAO) (1995), *FAO-UNESCO digital soil map of the world and derived soil properties*, U.N. Educ. Sci. Cultural Org., Paris.

Friesen, J., C. Rodgers, P. G. Oguntunde, J. M. H. Hendrickx, and N. van de Giesen (2008), Hydrotope-based protocol to determine average soil moisture over large areas for satellite calibration and validation with results from an observation campaign in the Volta Basin, West Africa, *IEEE Trans. Geosci. Remote Sensing*, *46*(7), 1995–2004.

Gharari, S., M. Hrachowitz, F. Fenicia, and H. H. G. Savenije (2011), Hydrological landscape classification: Investigating the performance of HAND based landscape classifications in a central European meso-scale catchment, *Hydrol. Earth Syst. Sci.*, *15*(11), 3275–3291.

Gu, R. R., and Y. Li (2002), River temperature sensitivity to hydraulic and meteorological parameters, *J. Environ. Manage.*, *66*(1), 43–56.

Guerschman, J. P., A. I. J. M. Van Dijk, G. Mattersdorf, J. Beringer, L. B. Hutley, R. Leuning, R. C. Pipunic, and B. S. Sherman (2009), Scaling of potential evapotranspiration with MODIS data reproduces flux observations and catchment water balance observations across Australia, *J. Hydrol.*, *369*, 107–119.

Habib, Z. (2004), Scope for reallocation of river waters for agriculture in the Indus Basin, Ph.D. dissertation, ENGREF, Montpellier, France.

Hargreaves, G. H., and Z. A. Samani (1985), Reference crop evapotranspiration from temperature, *Appl. Eng. Agric.*, *1*(2), 96–99.

Hemakumara, M., J. D. Kalma, J. P. Walker, and G. Willgoose (2004), Downscaling of low resolution passive microwave soil moisture observations, in *2nd International CAHMDA workshop on The Terrestrial Water Cycle: Modelling and Data Assimilation Across Catchment Scales*, edited by, A. J. Teuling et al., pp. 67–71, Wageningen University, Wageningen, Netherlands.

Hillel, D. (1998), *Environmental Soil Physics*, Academic Press, London, U.K.

Holtslag, A. A. M. (1984), Estimates of diabatic wind speed profiles from near-surface weather observations, *Boundary Layer Meteorol.*, *29*, 225–250.

Huffman, G. J., R. F. Adler, D. T. Bolvin, G. Gu, E. J. Nelkin, K. P. Bowman, Y. Hong, E. F. Stocker, and D. B. Wolff (2007), The TRMM Multisatellite Precipitation Analysis (TMPA): quasi-global, multiyear, combined-sensor precipitation estimates at fine scales, *J. Hydrometeorol.*, *8*, 38–55.

Immerzeel, W. W., and P. Droogers (2008), Calibration of a distributed hydrological model based on satellite evapotranspiration, *J. Hydrol.*, *349*, 411–424.

Jarvis, P. G. (1976), The interpretation of the variations in leaf water potential and stomatal conductance found in canopies in the field, *Philos. Trans. R. Soc. London B*, *273*(927), 593–610.

Jeevandas, A., R. P. Singh, and R. Kumar (2008), Concerns of groundwater depletion and irrigation efficiency in Punjab agriculture: A micro-level study, *Agric. Econ. Res. Rev.*, *21*, 191–199.

Jia, L., G. Xi, S. Liu, C. Huang, Y. Yan, and G. Liu (2009), Regional estimation of daily to annual regional evapotranspiration with MODIS data in the Yellow River Delta wetland, *Hydrol. Earth Syst. Sci.*, *13*, 1775–1787.

Jiang, Z., A. R. Huete, J. Chen, Y. Chen, J. Li, G. Yan, and X. Zhang (2006), Analysis of NDVI and scaled difference vegetation index retrievals of vegetation fraction, *Remote Sensing Environ.*, *101*(3), 366–378.

Kale, M., S. Singh, and P. S. Roy (2005), Estimation of leaf area index in dry deciduous forests from IRS-WiFS in central India, *Int. J. Remote Sensing*, *26*(21), 4855–4867.

Kalma, J. D., T. R. McVicar, and M. F. McCabe (2008), Estimating land surface evaporation: A review of methods using remotely sensed surface temperature data, *Surv. Geophys.*, *29*(4–5), 421–469.

King, M. D., S. C. Tsay, S. E. Platnick, M. Wang, and K. N. Liou (1997), Cloud retrieval algorithms for MODIS: Optical thickness, effective particle radius, and thermodynamic phase, *Rep. ATBD-MOD-05*, NASA Goddard Space Flight Cent., Greenbelt, MD, [available at http://modis atmos.gsfc.nasa.gov/_docs/atbd_mod05.pdf].

Kitchin, C. R. (1987), *Stars, Nebulae and the Interstellar Medium: Observational Physics and Astrophysics*, Adam Hilger, Bristol, U.K.

Li, F., W. P. Kustas, M. C. Anderson, T. J. Jackson, R. Bindlish, and J. H. Prueger (2006), Comparing the utility of microwave and thermal remote-sensing constraints in two-source energy balance modeling over an agricultural landscape, *Remote Sensing Environ.*, *101*(3), 315–328.

Lillesand, T., and R. W. Kiefer (2000), *Remote Sensing and Image Interpretation*, John Wiley and Sons, New York.

Long, D., and V. P. Singh (2012), A modified surface energy balance algorithm for land (M-SEBAL) based on a trapezoidal framework, *Water Resour. Res.*, *48*, W02528, doi:10.1029/2011WR010607.

Mehrez, M. B., O. Taconet, D. Vidal-Madjar, and C. Valencogne (1992), Estimation of stomatal resistance and canopy evaporation during the HAPEX-MOBILHY experiment, *Agric. For. Meteorol.*, *58*(3–4), 285–313.

Meijninger, W. M. L., O. K. Hartogensis, W. Kohsiek, J. C. B. Hoedjes, R. M. Zuurbier, and H. A. R. De Bruin (2002), Determination of area-averaged sensible heat fluxes with a large aperture scintillometer over a heterogeneous surface-Flevoland field experiment, *Boundary Layer Meteorol.*, *105*(1), 37–62.

Merlin, O., A. Chehbouni, Y. H. Kerr, and D. C. Goodrich (2006), A downscaling method for distributing surface soil moisture within a microwave pixel: Application to the Monsoon '90 data, *Remote Sensing Environ.*, *101*, 379–389.

Merlin, O., A. Chehbouni, J. P. Walker, R. Panciera, and Y. H. Kerr (2008), A simple method to disaggregate passive microwave-based soil moisture, *IEEE Trans. Geosci. Remote Sensing*, *46*(3), 786–796.

Mizoguchi, Y., A. Miyata, Y. Ohtani, R. Hirata, and S. Yuta (2009), A review of tower flux observation sites in Asia, *J. For. Res.*, *14*(1), 1–9.

Molden, D. J., and R. Sakthivadivel (1999), Water accounting to assess use and productivity of water, *Int. J. Water Resour. Dev.*, *15*(1–2), 55–71.

Monteith, J. L. (1981), Evaporation and surface temperature, *Q. J. R. Meteorol. Soc.*, *107*(451), 1–27.

Mu, Q., F. A. Heinsch, M. Zhao, and S. W. Running (2007), Development of a global evapotranspiration algorithm based on MODIS and global meteorology data, *Remote Sensing Environ.*, *11*, 519–536.

Nagler, P. L., R. L. Scott, C. Westenburg, J. R. Cleverly, E. P. Glenn, and A. R. Huete (2005), Evapotranspiration on western U.S. rivers estimated using the Enhanced Vegetation Index from MODIS and data from eddy covariance and Bowen ratio flux towers, *Remote Sensing Environ.*, *97*(3), 337–351.

New, M., M. Hulme, and P. Jones (1999), Representing twentieth-century space–time climate variability. Part 1: Development of a 1961–90 mean monthly terrestrial climatology, *J. Clim.*, *12*(3), 829–856.

Njoku, E. G. (2008), *AMSR-E/Aqua Daily L3 Surface Soil Moisture, Interpretive Parameters, and QC EASE-Grids V002*, January to December 2007, Natl. Snow Ice Data Cent., Boulder, Colo.

Pakistan Agricultural Research Council (PARC) (1982), *Consumptive use of water for crops in Pakistan*, pp. 20–30, Islamabad, Pakistan.

Perry, C. (2007), Efficient irrigation; inefficient communication; flawed recommendations, *Irrig. Drain.*, *56*, 367–378.

Pitman, A. J. (1994), Assessing the sensitivity of a land-surface scheme to the parameter values using a single column model, *J. Clim.*, *7*(12), 1856–1869.

Price, J. C. (1990), Using spatial context in satellite data to infer regional scale evapotranspiration, *IEEE Trans. Geosci. Remote Sensing*, *28*(5), 940–948.

Qureshi, A. S., P. G. McCornick, A. Sarwar, and B. R. Sharma (2010), Challenges and prospects of sustainable groundwater management in the Indus Basin, Pakistan, *Water Resour. Manage.*, *24*, 1551–1569.

Radersma, S., and N. de Ridder (1996), Computed evapotranspiration of annual and perennial crops at different temporal and spatial scales using published parameter values, *Agric. Water Manage.*, *31*(1–2), 17–34.

Sarwar, A., and W. G. M. Bastiaanssen (2001), Long-term effects of irrigation water conservation on crop production and environment in semiarid areas, *J. Irrig. Drain. Eng.*, *127*(6), 331–338.

Sarwar, A., and R. Bill (2007), Mapping evapotranspiration in the Indus Basin using ASTER data, *Int. J. Remote Sensing*, *28*(22), 5037–5046.

Sarwar, A., and H. Eggers (2006), Development of a conjunctive use model to evaluate alternative management options for surface and groundwater resources, *Hydrogeol. J.*, *14*(8), 1676–1687.

Schulze, R. E., G. A. Kiker, and R. P. Kunz (1993), Global climate change and agricultural productivity in southern Africa, *Global Environ. Change*, *3*(4), 330–349.

Seckler, D. (1996), *The new era of water resources management: From "dry" to "wet" water savings*, Int. Water Manage. Inst., Colombo, Sri Lanka.

Seckler, D., R. Barker, and U. Amarasinghe (1999), Water scarcity in the twenty-first century, *Int. J. Water Resour. Dev.*, *15*(1–2), 29–42.

Senay, G. B., M. Budde, J. P. Verdin, and A. M. Melesse (2007), A coupled remote sensing and simplified surface energy balance approach to estimate actual evapotranspiration from irrigated fields, *Sensors*, *7*, 979–1000.

Shah, T., D. J. Molden, R. Sakthivadivel, and D. Seckler (2000), The global groundwater situation: Overview of opportunities and challenges, report, Int. Water Manage. Inst., Colombo, Sri Lanka.

Shakir, A. S., N. M. Khan, and M. M. Qureshi (2010), Canal water management: Case study of upper Chenab Canal in Pakistan, *Irrig. Drain.*, *59*(1), 76–91.

Shakoor, A., A. Shehzad, and M. N. Asghar (2006), Application of remote sensing techniques for water resources planning and management, in *International Conference on Advances in Space Technologies*, pp. 142–146, Inst. of Electr. and Electron. Engin., Washington, DC.

Sharma, M. L. (1985), *Estimating Evapotranspiration, Adv. Irrig.*, vol. 3, Academic Press, Orlando, Fla.

Shuttleworth, W. J., and J. S. Wallace (1985), Evaporation from sparse crops-an energy combination theory, *Q. J. R. Meteorol. Soc.*, *111*(469), 839–855.

Stewart, J. B. (1988), Modelling surface conductance of pine forest, *Agric. For. Meteorol.*, *43*(1), 19–35.

Tang, Q., S. Peterson, R. H. Cuenca, Y. Hagimoto, and D. P. Lettenmaier (2009), Satellite-based near-real-time estimation of irrigated crop water consumption, *J. Geophys. Res.*, *114*, D05114, doi:10.1029/2008JD010854.

Teixeira, D. C. A., and W. G. M. Bastiaanssen (2012), Five methods to interpret field measurements of energy fluxes over a micro-sprinkler-irrigated mango orchard, *Irrig. Sci.*, *30*(1), 13–28.

Thornton, P. E., S. W. Running, and M. A. White (1997), Generating surfaces of daily meteorological variables over large regions of complex terrain, *J. Hydrol.*, *190*, 214–251.

Twine, T. E., W. P. Kustas, J. M. Norman, D. R. Cook, P. R. Houser, T. P. Meyers, J. H. Prueger, P. J. Starks, and M. L. Wesely (2000), Correcting eddy-covariance flux underestimates over a grass land, *Agric. For. Meteorol.*, *103*, 279–300.

Ulaby, F. T., R. K. Moore, and A. K. Fung (1981), *Microwave Remote Sensing: Active and Passive*, Artech House, Dedham, Mass.

Vanderkimpen, P. J. (1991), Estimation of crop evapotranspiration by means of the Penman-Monteith equation, Ph.D. dissertation, Dep. of Biol. and Irrig. Eng., Utah State Univ., Logan, Utah.

van Genuchten, M. T. (1980), A closed-form equation for predicting the hydraulic conductivity of unsaturated soils, *Soil Sci. Soc. Am. J.*, *44*, 892–898.

von Hoyningen-Hune, J. (1983), Die interception des niederschlags in landwirtschaftlichen bestanden, *Schriftenr. DVWK*, *57*, 1–53.

Wallace, J. S., J. H. C. Gash, D. D. McNeil, and M. V. K. Sivakumar (1986), Measurement and prediction of actual evaporation from sparse dryland crops-scientific report on Phase II of ODA Project 149, *ODA Rep., OD 149/3*, 59 pp., Inst. of Hydrol., Wallingford, UK.

Wu, B., N. Yan, J. Xiong, W. G. M. Bastiaanssen, W. Zhu, and A. Stein (2012), Validation of ETWatch using field measurements at diverse landscapes: A case study in Hai Basin of China, *J. Hydrol.*, *436–437*, 67–80, doi:10.1016/j.jhydrol.2012.1002.1043.

Zwart, S. J., W. G. M. Bastiaanssen, C. de Fraiture, and D. J. Molden (2010), WATPRO: A remote sensing based model for mapping water productivity of wheat, *Agric. Water Manage.*, *97*(10), 1628–1636.